Chapter 3

Design for manufacture of Fabry-Perot cavity sensors

When Fabry-Perot cavity sensors are manufactured, the thickness of each layer must be tightly controlled to achieve the target performance of a sensor. However, there are unavoidable errors in thickness even though techniques of thickness control for thin films have rapidly improved [1] . For Fabry-Perot optical interference filters it has long been recognized that the performance of the filter is greatly influenced by random thickness variations in the films. For instance, the resonant wavelength is very sensitive to thickness variations. Degradation in the performance of the filters has been simulated by Monte Carlo technique or analytic methods [2, 3] .

In this chapter the impact of manufacturing-induced variations on the performance of Fabry-Perot cavity sensors is studied. In particular, we consider how random variations in thickness of the cavity mirrors influence the accuracy with which gap can be measured. Through the study, it is found that there exists an optimum design of a Fabry-Perot cavity sensor, which is a combination of initial cavity gap and mechanical travel of the moving mirror. The optimum design gives large manufacturing tolerance to the thickness variations of layers and it leads to high accuracy.

3.1   IMPACT OF THICKNESS VARIATIONS ON OPTICAL RESPONSE

In this section, the variation of the optical response, e.g., of reflectance, due to the thickness variation of the layers is calculated using an analytic method. This calculation will be a basis for designing Fabry-Perot sensors for manufacture, which is to be discussed in the following section. The first derivative of the reflectance (R) with respect to the thickness of the ith layer can be calculated by using the first derivative of the equivalent characteristic matrix (M). From equation (2.4)

$$\frac{\partial R}{\partial z_i} = \left(\frac{\partial}{\partial z_i} P\right) \cdot P^* + P \cdot \left(\frac{\partial}{\partial z_i} P^*\right),$$

(3.1)

where $P = \dfrac{\eta_{in} B - C}{\eta_{in} B + C}$ and P^* is the conjugate of P. The partial derivatives of B and C are calculated from

$$\frac{\partial}{\partial z_i}\begin{bmatrix} B \\ C \end{bmatrix} = \frac{\partial}{\partial z_i} M \cdot \begin{bmatrix} 1 \\ \eta_f \end{bmatrix}.$$

(3.2)

The first derivative of the equivalent characteristic matrix is obtained using equation (2.3)

$$\frac{\partial M}{\partial z_i} = M_q \cdot M_{q-1} \cdots \frac{\partial M_i}{\partial z_i} \cdots M_1,$$

(3.3)

where $\dfrac{\partial M_i}{\partial z_i} = k_o n_i \begin{pmatrix} -\sin(k_o\, n_i\, z_i) & \dfrac{j}{\eta_i}\cos(k_o\, n_i\, z_i) \\ j\, \eta_i \cos(k_o\, n_i\, z_i) & -\sin(k_o\, n_i\, z_i) \end{pmatrix}.$

Using equations (3.1), (3.2) and (3.3), the first derivatives of the reflectance of a Fabry-Perot cavity with respect to each layer can be calculated.

For the Fabry-Perot cavity sensors described in chapter 2, the first derivatives of the reflectances with respect to each layer are calculated as a function of gap. Figure 3.1 shows a plot of the first derivative of the reflectance of the Fabry-Perot cavity with metal (Au) mirrors. The mirrors of the cavity are numbered in ascending order from the fiber, for convenience. From the figure, it is obvious that the reflectance of the cavity is the most sensitive to the thickness variation of the first Au layer which the incident light meets. Thus, thickness control of the first Au layer would be very critical to achieve a target reflectance of the cavity.

As shown in equation (3.3), the first derivative of reflectance with respect to a layer also depends on the refractive index of the layer. It implies that for a given thickness variation the reflectance curve would be more perturbed by thickness variation of a layer with larger refractive index. Figure 3.2 plots the first derivatives of the reflectance of a Fabry-Perot cavity with dielectric mirrors as described in chapter 2. Each dielectric layer is numbered in ascending order from the fiber. For example, nitride 2 represents the second silicon nitride layer which the incident light meets. Comparing Figure 3.1 with Figure 3.2, it should be noted that the magnitudes of the derivatives with respect to the dielectric layers, i.e., silicon dioxide and silicon nitride, are much smaller than ones with respect to the metal layers (Au). This indicates that a film with small refractive index would be preferred as a mirror layer if manufacturing process for the film

21

produces the same process-induced thickness variation as a film with large

refractive index, assuming the layers were of equal thickness.
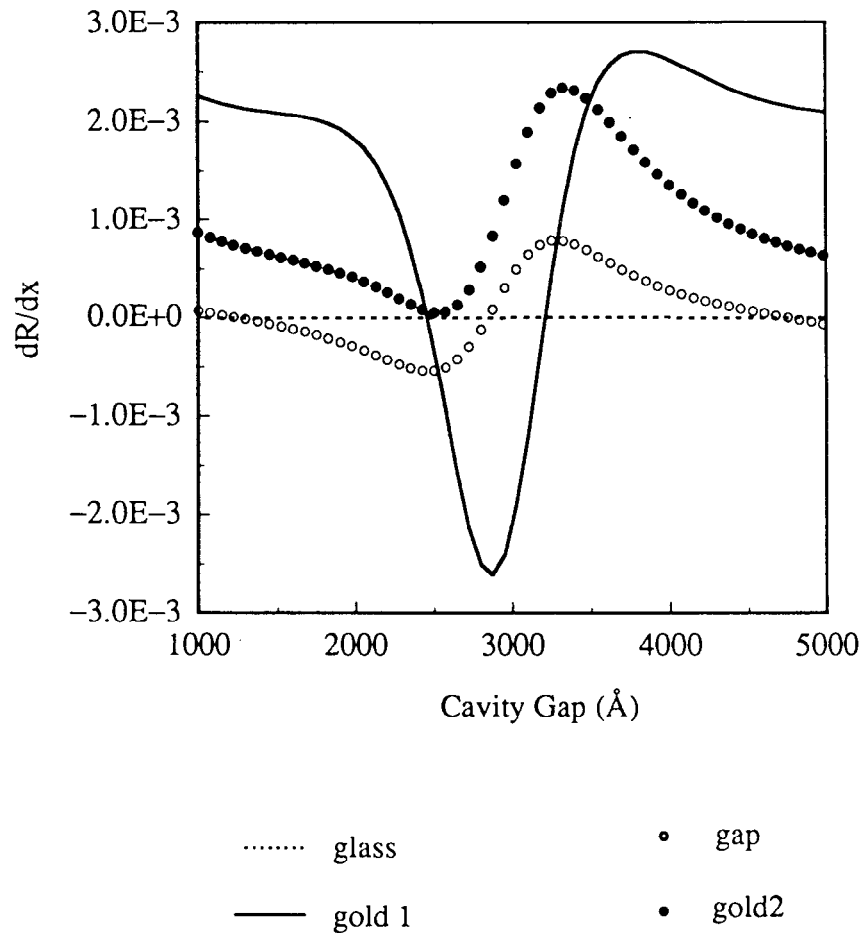
Figure 3.1 : The first derivatives of the reflectance of a Fabry-Perot cavity with metal (Au) mirrors, as shown in Figure 2.5. The vertical axis represents the first derivative of the reflectance of the cavity with respect to the thickness of each layer.
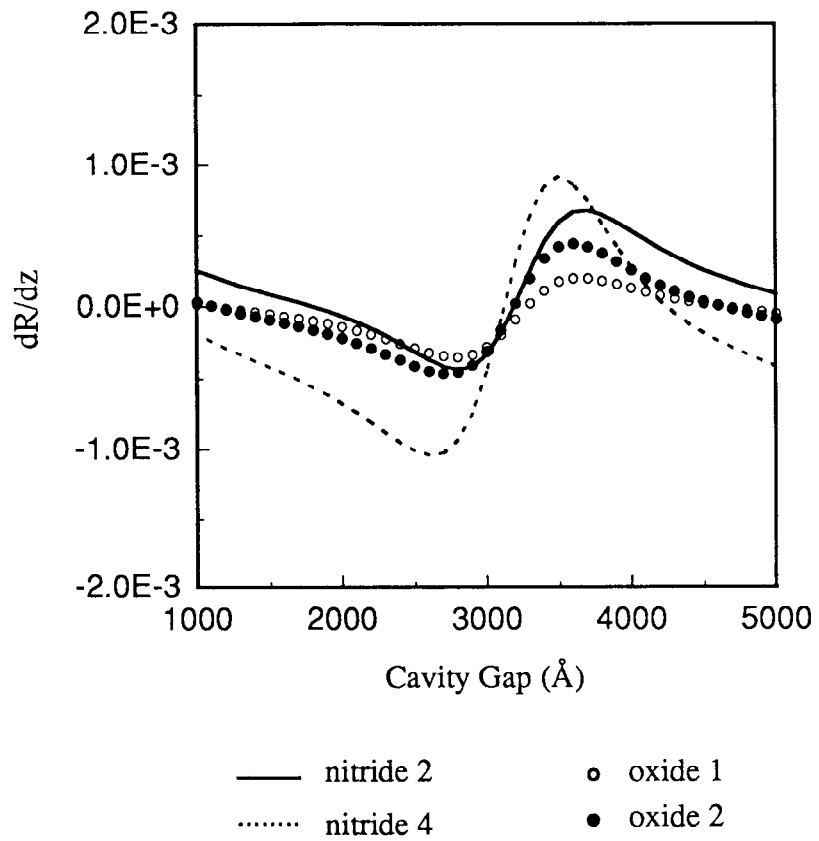
Figure 3.2 : The first derivatives of the reflectance of a Fabry-Perot cavity with dielectric films, as shown in Figure 2.6. For simplicity, only the four layers with the largest derivatives are shown.

3.2   DESIGN METHODOLOGY AND CASE STUDY FOR MANUFACTURE

If Fabry-Perot sensors are to be manufactured in large volume at low cost, it will not be practical to individually calibrate every sensor to eliminate fabrication-induced response variations. Instead of calibrating every sensor, it would be preferable if a nominal response curve could be given for a set of the manufactured sensors with some specified accuracy. The accuracy is limited by the amount of change in the response curve due to the thickness variation of the layers.

Quantitative treatment of the accuracy of a design is discussed in the following subsections. Using the first derivatives obtained in the last section, uncertainty in gap induced by thickness variation can be calculated and included in the calculation of accuracy. Finally, the accuracy can be used as a metric to find an optimum design for manufacture of Fabry-Perot cavity sensors.

3.2.1   Design Methodology

For Fabry-Perot sensors, the cavity gap g could be inferred from some measurement of reflected light intensity **I**, that is a function of the reflectance **R**, that is in turn a function of wavelength and the structure of the sensor. For example, absolute reflectance of the cavity could be used as a measurand as done in chapter 2. The detection scheme is, however, very susceptible to any light intensity change in the fiber due to coupling and fiber bending. As an alternative, a ratio of the reflectances at two wavelengths (λ_1 and λ_2) could be used as a measurand. Such a detection scheme will be called the dual wavelength

technique in this chapter. This method eliminates errors resulting from wavelength-independent changes in the fiber interconnect to the sensor, such as fiber bending loss and coupling loss.

Taking manufacturing-induced variations of layer thickness into account, it should be realized that a given measurand value $\mathbf{I}(\boldsymbol{R}, \lambda)$ could be produced from a Fabry-Perot cavity which has different layer thicknesses from a target design. This leads to an error in estimating the cavity gap g. In other words, there exists an uncertainty Δg in the gap at a given measurand $\mathbf{I}(\boldsymbol{R}, \lambda)$ since for mirror layers with thicknesses $\left(z_1 + \Delta z_1, z_2 + \Delta z_2, \cdots, z_q + \Delta z_q\right)$ there can exist a gap thickness $g + \Delta g$ that would produce an identical value of $\mathbf{I}$

$$\mathbf{I}\left[\boldsymbol{R}\left(z_1, z_2, \cdots, g, \cdots, z_q, \lambda\right)\right] = \mathbf{I}\left[\boldsymbol{R}\left(z_1 + \Delta z_1, z_2 + \Delta z_2, \cdots, g + \Delta g, \cdots, z_q + \Delta z_q, \lambda\right)\right] \quad (3.4)$$

where the functional dependencies of $\boldsymbol{R}$ have been indicated explicitly.

In principle, it should be possible to obtain Δg by calculating the response for all possible thickness combinations weighted by the distribution functions representing the process-induced thickness variation of each layer. This approach is computationally impractical when q becomes large (for instance, if the cavity mirrors are made using multilayer dielectric mirrors).

The uncertainty Δg in gap can be analytically expressed using a Taylor series approximation

$$\mathbf{I}\left[\mathbf{R}\left(z_1 + \Delta z_1, z_2 + \Delta z_2, \cdots, g + \Delta g, \cdots, z_q + \Delta z_q, \lambda\right)\right]$$

$$\approx \mathbf{I}\left[\mathbf{R}\left(z_1, z_2, \cdots, g, \cdots, z_q, \lambda\right)\right] + \sum_{\substack{i=1 \\ i \neq k}}^{q} \left\{\frac{\partial \mathbf{I}}{\partial z_i}\right\} \cdot \Delta z_i + \left\{\frac{\partial \mathbf{I}}{\partial g}\right\} \cdot \Delta g \quad . \tag{3.5}$$

Combining equations (3.4) and (3.5) then gives Δg;

$$\Delta g \approx -\left[\left(\frac{\partial \mathbf{I}}{\partial g}\right)\right]^{-1} \cdot \sum_{\substack{i=1 \\ i \neq k}}^{q} \Delta z_i \cdot \left(\frac{\partial \mathbf{I}}{\partial z_i}\right). \tag{3.6}$$

To bound the uncertainty in gap, we should find the combination of layer thicknesses that maximizes Δg for a given set of Δz_i; examination of equation (3.6) gives this bound, Δg_{proc}, as

$$\Delta g_{proc} = \left|\frac{\partial \mathbf{I}}{\partial g}\right|^{-1} \sum_{\substack{i=1 \\ i \neq k}}^{q} \left|\left\{\frac{\partial \mathbf{I}}{\partial z_i}\right\} \cdot \Delta z_i\right| \quad . \tag{3.7}$$

In terms of yield, if for each mirror layer i ($i \neq k$) the fraction of devices with thickness between $z_i - \Delta z_i$ and $z_i + \Delta z_i$ is P_i, then for a fixed value of $\mathbf{I}(\mathbf{R}, \lambda)$, the fraction of sensors $P_{\Delta g}$ with gap between $g - \Delta g_{proc}$ and $g + \Delta g_{proc}$ that would produce this value of $\mathbf{I}(\mathbf{R}, \lambda)$ would be at least

$$P_{\Delta g} = \prod_{\substack{i=1 \\ i \neq k}}^{q} P_i \quad . \tag{3.8}$$

To further specify the performance of the Fabry-Perot sensor quantitatively, the operational range for the device must be specified. Here we assume two primary design space variables: i) the initial gap g_i of the Fabry-Perot

cavity; and ii) the maximum mechanical travel t of the moving mirror. The second variable, t, is determined by the maximum stimulus (e.g., the maximum pressure) and the mechanical compliance of the membrane supporting the moving mirror. Since mechanical compliance frequently can be adjusted independently of the thicknesses of the mirror layers by changing the lateral size, t is considered a freely adjustable design variable. Over the full range of stimuli, g varies between g_i and $g_i - t$, assuming the stimulus generates a motion of the mirror which decreases the cavity gap. Also, Δg_{proc} varies since Δg_{proc} is a function of g. We are now ready to see how uncertainty Δg_{proc} in the gap influences the accuracy of the sensor: since the maximum stimulus corresponds to the maximum travel t, the percentage accuracy would be bounded by the maximum value of Δg_{proc} in the interval between g_i and $g_i - t$, divided by t.

For example, if one wishes to find the accuracy [4] for a given nominal initial gap g_i and travel t, including the uncertainties induced by thickness variations in mirror layers, one must find the error ε^o_{proc}

$$\varepsilon^o_{proc} = \mathbf{max} \left\{ \frac{\Delta g_{proc}}{t} : g \in \left[g_i - t, \ g_i \right] \right\} . \tag{3.9}$$

The best design (i.e., the best values of g_i and t) is the one that minimizes ε^o_{proc}. However, it should be remembered that manufacturing uncertainty in layer thickness also includes the process that determines the initial gap g_i. Even if one assumes a single calibration measurement is made to determine the specific value of g_i for a given manufactured sensor, the overall design should still allow g_i to vary over the range $g_i \cdot (1 \pm \delta)$, where δ is the normalized thickness variation for the gap layer. Thus, the accuracy defined by equation (3.9) must be modified to

$$\varepsilon_{proc} = \mathbf{max} \left\{ \frac{\Delta g_{proc}}{t} : g \in \left[g_i \cdot (1 - \delta) - t \, , \, g_i \cdot (1 + \delta) \right] \right\} . \qquad (3.10)$$

The best design, taking uncertainties in the thickness of all layers into account, is the one that minimizes ε_{proc}.

In terms of yield, if the fraction of sensors with actual gap in the range $g_i \cdot (1 \pm \delta)$ is P_k, then the fraction of sensors P with accuracy not worse than ε_{proc} is at least

$$P = P_k \cdot P_{\Delta g} \qquad (3.11)$$

In addition to the process-induced errors, one could include errors from fitting the actual measurand $\mathbf{I}(R, \lambda)$ with a fitting function g_{fit}. Since it is usually not possible to analytically invert the function $\mathbf{I}(R)$ to find g, a common approach is to find a fitting function $g_{fit}(\mathbf{I})$ to relate the gap g to the actual measurand $\mathbf{I}$. Assuming all the mirror layers take on their nominal thicknesses, using equations (2.2)-(2.4) we can find $\mathbf{I}(g)$ exactly. The difference between the exact relationship and the fitting function is then Δg_{fit}

$$\Delta g_{fit} = \left| g_{fit} \left[\mathbf{I}(g) \right] - g \right| . \qquad (3.12)$$

If one wishes to find a fitting function that gives the best accuracy for a given initial gap g_i and travel t, we must choose a fitting function so that the error ε_{fit}

$$\varepsilon_{fit} = \mathbf{max} \left\{ \frac{\Delta g_{fit}}{t} : g \in \left[g_i - t, \, g_i \right] \right\} \qquad (3.13)$$

is minimized.

Note that the fitting function g_{fit} minimizing equation (3.13) is different from the least squares fitting function g_{least} , which minimizes ε_{least}

$$\varepsilon_{least} = \left\{ \sum_g \left| g_{least}[\mathbf{I}(g)] - g \right|^2 : g \in [g_i - t, g_i] \right\} .$$
(3.14)

Comparing the definitions of the two fitting functions, g_{fit} would give better accuracy than g_{least}.

If both fitting and process-induced errors are included, the design that would give the best accuracy is one where the total error ε_{tot}

$$\varepsilon_{tot} = \mathbf{max} \left\{ \frac{\Delta g_{fit} + \Delta g_{proc}}{t} : g \in [g_i \cdot (1 - \delta) - t , g_i \cdot (1 + \delta)] \right\}$$
(3.15)

is minimized.

3.2.2 Example Designs

To illustrate a design process, the measurand $\mathbf{I}(R, \lambda)$ must be specified. If reflectance of the cavity at a single wavelength λ_1 is used as the measurand,

$$\mathbf{I}\Big[R\big(z_1, z_2, \cdots, g, \cdots, z_q, \lambda\big)\Big] = R\big(z_1, z_2, \cdots, g, \cdots, z_q, \lambda_1\big) \quad . \tag{3.16}$$

This response curve will be periodic in g, with period $\lambda_1/2$ and equation (3.7) becomes

$$\Delta g_{proc} = \left|\frac{\partial \mathbf{R}}{\partial g}\right|^{-1} \sum_{\substack{i=1 \\ i \neq k}}^{q} \left|\left\{\frac{\partial \mathbf{R}}{\partial z_i}\right\} \cdot \Delta z_i\right| \quad , \tag{3.17}$$

where $\mathbf{R}$ can be found using the method discussed in chapter 2.

Figure 3.3 shows reflectance and Δg_{proc} of a Fabry-Perot sensor with metal (Au) mirrors described in the chapter 2. The periodicity of the curve suggests two basic operating branches, one between 100 nm and 275 nm, and the other between 275 nm and 450 nm. Using equation (3.17) Δg_{proc} was calculated, assuming thickness variation Δz for the Au layers is ± 3 Å (three sigma), which can be achieved with thin film coating equipment.

For comparison, extensive random combinations of Au mirror thickness from 67 Å to 73 Å have been tested to verify that for a given reflectance R the maximum change in g is produced by the perturbed layer thicknesses used in equation (3.7). Agreement between the two approaches indicates that the first order Taylor series approximation used in equation (3.5) is sufficient for this case.
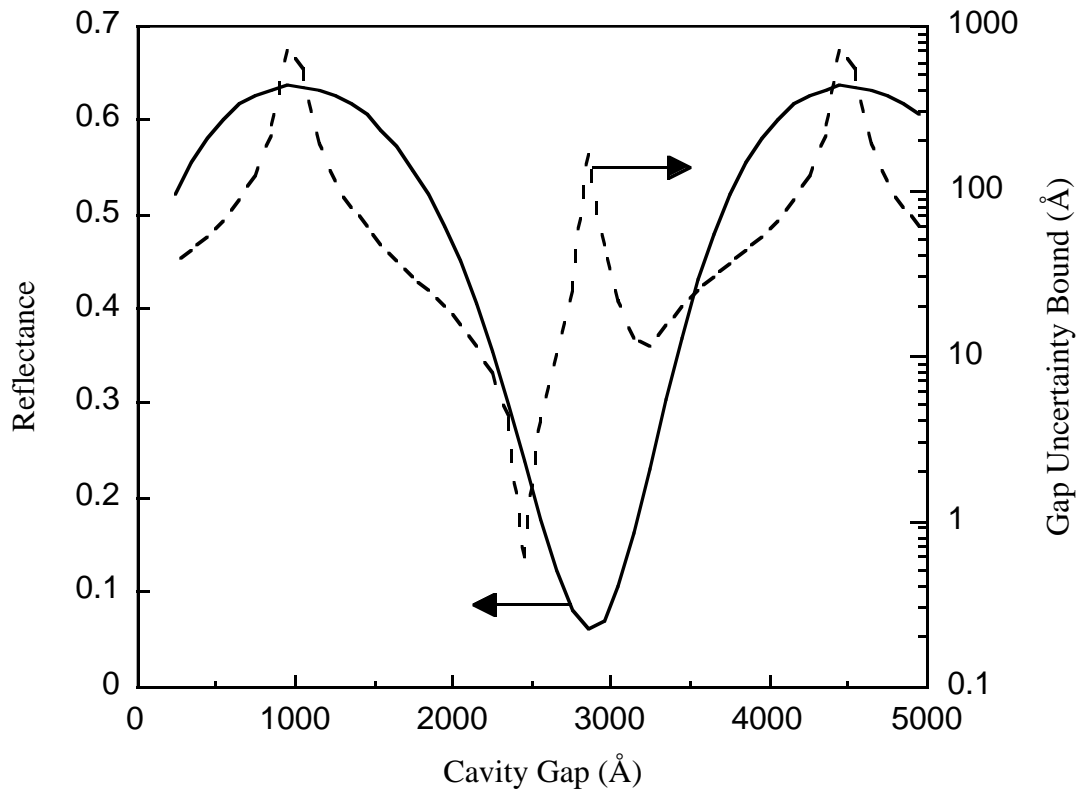
Figure 3.3 : Reflectance and process-induced response variations of a Fabry-Perot cavity with Au mirrors for a single wavelength (lambda = 700 nm). Solid line: reflectance; Dotted line: bound on gap uncertainty $\Delta g_{proc.}$

For dielectric mirrors, the variation in thickness of each layer was assumed to be ±3% of the nominal thickness. State-of-the-art deposition or sputtering technology can provide ±3% variation in thickness with ±3σ process tolerance [5, 6]. Figure 3.4 shows a plot of reflectance and Δg_{proc} of the Fabry-Perot cavity with the dielectric layers described in the chapter 2. Even though the dielectric layers show the smaller first derivatives as shown in Figure 3.2, the maximum uncertainty in the gap (Δg_{proc}) is much bigger than one with metal mirrors. The

bigger maximum uncertainty is caused by thickness variation, which is proportional to the nominal thickness of the dielectric layers, as indicated in equation (3.17).
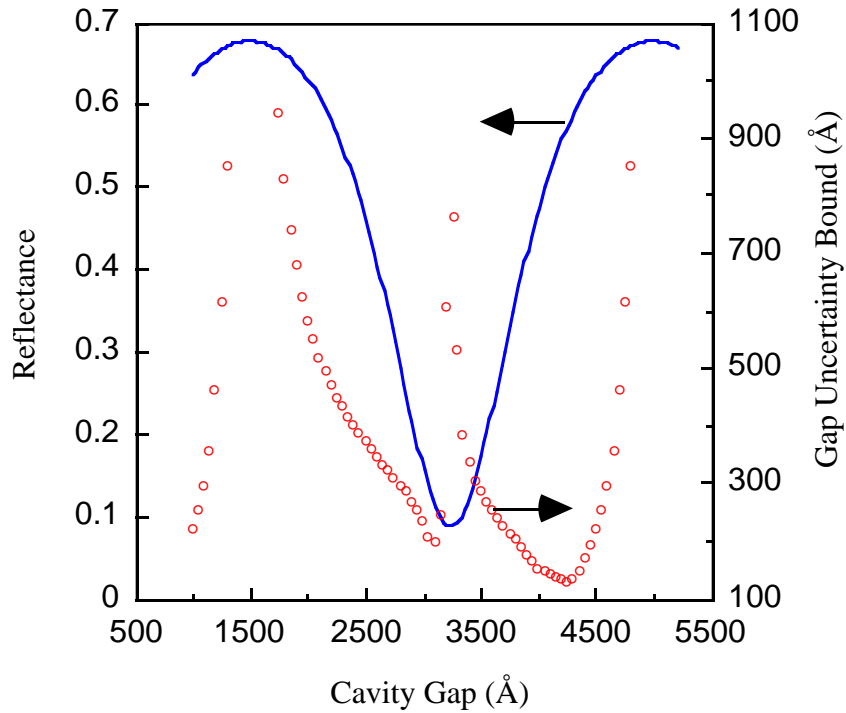
Figure 3.4 : Reflectance and process-induced response variations of a Fabry-Perot cavity with dielectric mirrors for a single wavelength (lambda = 700 nm). Solid line: reflectance; Dotted line: bound on gap uncertainty $\Delta g_{proc.}$

Note that for both the Fabry-Perot cavities the process-induced error Δg_{proc} in one branch is smaller than in the other. This implies that although the response curves for the two branches are almost identical, their sensitivity to layer thickness variations is not.

To find an optimum design which produces the best accuracy contour maps can be generated over the design space, i.e., for each choice of nominal initial gap g_i and maximum mechanical travel t. For simplicity, we first assume it is desirable to find a design that produces the best accuracy when the only errors are due to layer thickness variations (i.e., we use a "high order" fitting function so that $\Delta g_{fit} = 0$). Equation (3.10) is then used to find ε_{proc} for each possible design and contours of constant accuracy are plotted against g_i and t. As an illustration contour maps are generated for the case of metal mirrors because Δg_{proc} of dielectric mirrors is much worse than one of metal mirrors as shown in Figure 3.4 and Figure 3.3.

Figure 3.5 shows these contours for the case where the measurand is the single wavelength reflectance of the Fabry-Perot cavity with metal (Au) mirrors. For instance, 5 % accuracy could be achieved for a range of designs with g_i between about 2470 Å and 2700 Å, with corresponding travel between about 200 Å and 1200 Å. The fraction of devices with accuracy not worse than the contour value is given by equation (3.11); since we have used three sigma values for the layer thickness variations ($P_i = 0.99$), and there are three layers in this example (two metal mirrors plus the sacrificial layer), the fraction of sensors P with accuracy not worse than ε_{proc} is $[0.99]^3$, i.e., at least 97 %.
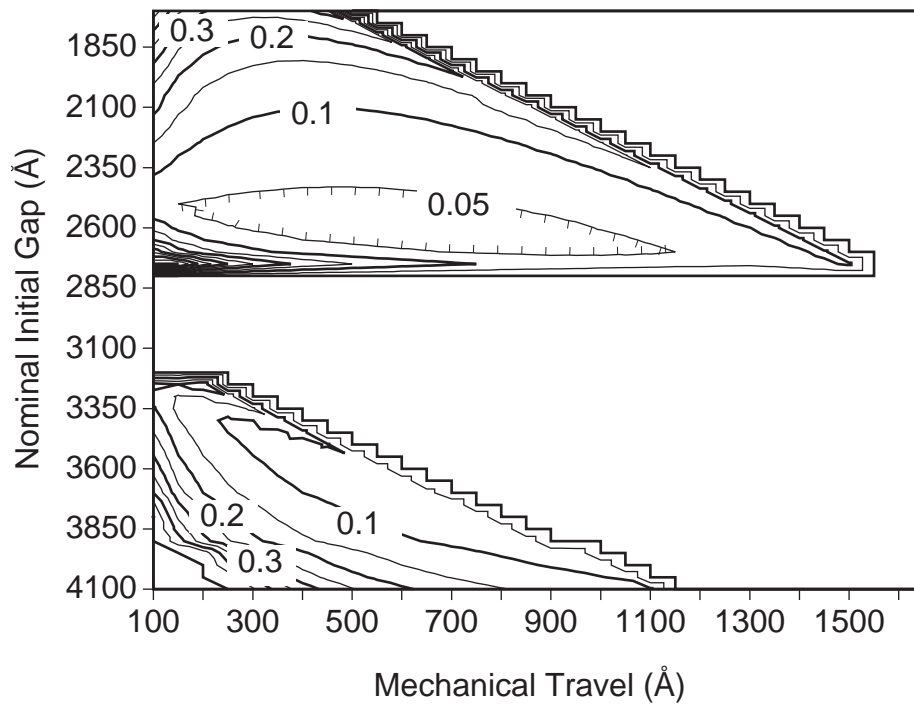
Figure 3.5 : Contour map over design space (i.e. initial gap and mechanical travel) when only process-induced thickness variations are considered. The numbers on the contour lines represent the accuracy of corresponding designs.

Figure 3.6 shows contours for the case where there is only fitting error. A linear fitting function defined in equation (3.13) is assumed. Finally, Figure 3.7 shows the accuracy contour plot assuming that both process-induced variations and linear fitting errors are included. Not surprisingly, the range of travels that can still give 5 % accuracy is considerably reduced, with an optimum design at g_i $\approx$ 2600 Å and $t \approx$ 300 Å. With this design at least 97 % of the manufactured sensors would give 5 % accuracy or better.
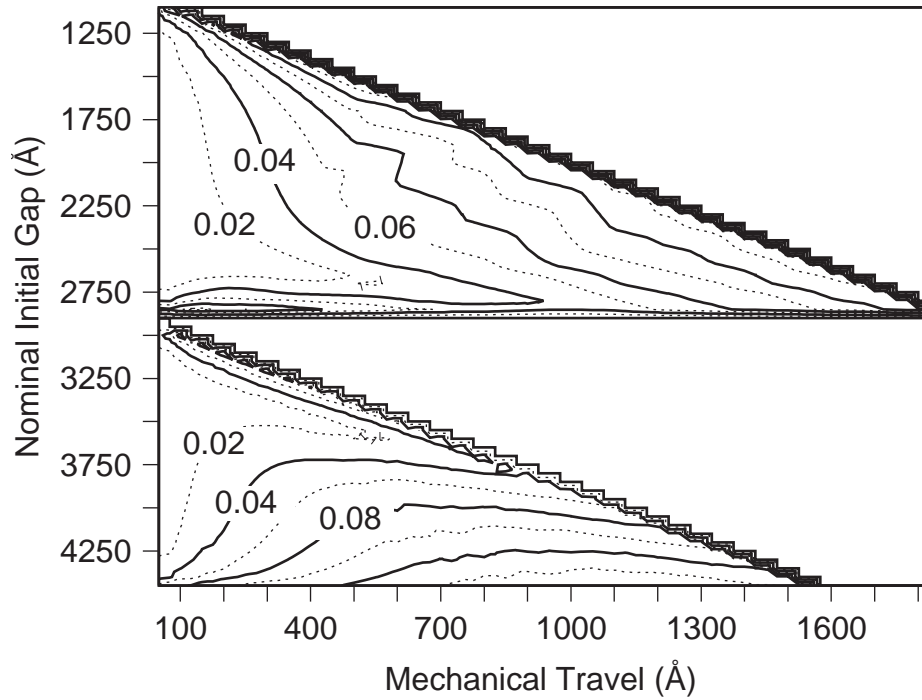
Figure 3.6 : Accuracy contour map, including only linear fitting errors, for single wavelength detection. Numbers on lines represent the accuracy of the contour.
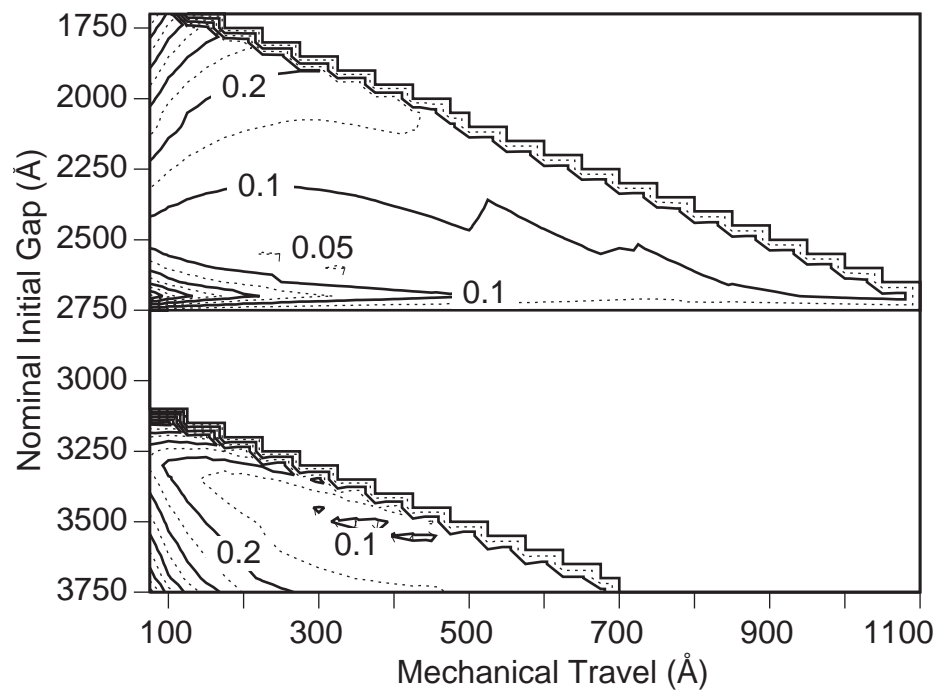
Figure 3.7 : Accuracy contour map, including both mirror variations and linear fitting errors, for single wavelength detection.

This design process can be applied to the case where another measurand is chosen. Suppose a ratio of two reflectances at different wavelengths λ_1 and λ_2 is used as a measurand. The following equation is one of the possible ratiometric methods

$$\mathbf{I}(\mathbf{R}) = \frac{\mathbf{R}(\lambda_1)}{\mathbf{R}(\lambda_1) + \mathbf{R}(\lambda_2)} \quad . \tag{3.18}$$

Substituting $\mathbf{I}(\mathbf{R}, \lambda)$ in equation (3.7) with equation (3.18), Δg_{procs} becomes

$$\Delta g_{procs} = \frac{\sum\limits_{\substack{i=1 \\ i \neq k}}^{q} \left| \left(\mathbf{R}_2 \frac{\partial \mathbf{R}_1}{\partial z_i} - \mathbf{R}_1 \frac{\partial \mathbf{R}_2}{\partial z_i} \right) \cdot \Delta z_i \right|}{\left| \mathbf{R}_1 \frac{\partial \mathbf{R}_2}{\partial g} - \mathbf{R}_2 \frac{\partial \mathbf{R}_1}{\partial g} \right|}. \tag{3.19}$$

Figure 3.8 shows the response curve and associated process-induced errors of the cavity with metal (Au) mirrors for dual wavelength detection, assuming detection wavelengths of 560 nm and 700 nm. The response curve is still a periodic function with respect to gap, but with a period equal to the lowest common multiple of $\frac{\lambda_1}{2}$ and $\frac{\lambda_2}{2}$. There are now nine distinct operating branches. Note that the process-induced errors in the branch from 8000 Å to 10000 Å are smaller than any other regions.

Figure 3.9 shows contour maps including only process-induced errors. The two best branches are chosen which have smaller process-induced errors than any other branches as shown in Figure 3.8. The maps suggest an optimum design for g_i = 9325 Å and t = 825 Å, with at least 97 % of the sensors producing an accuracy of not worse than 1 %.
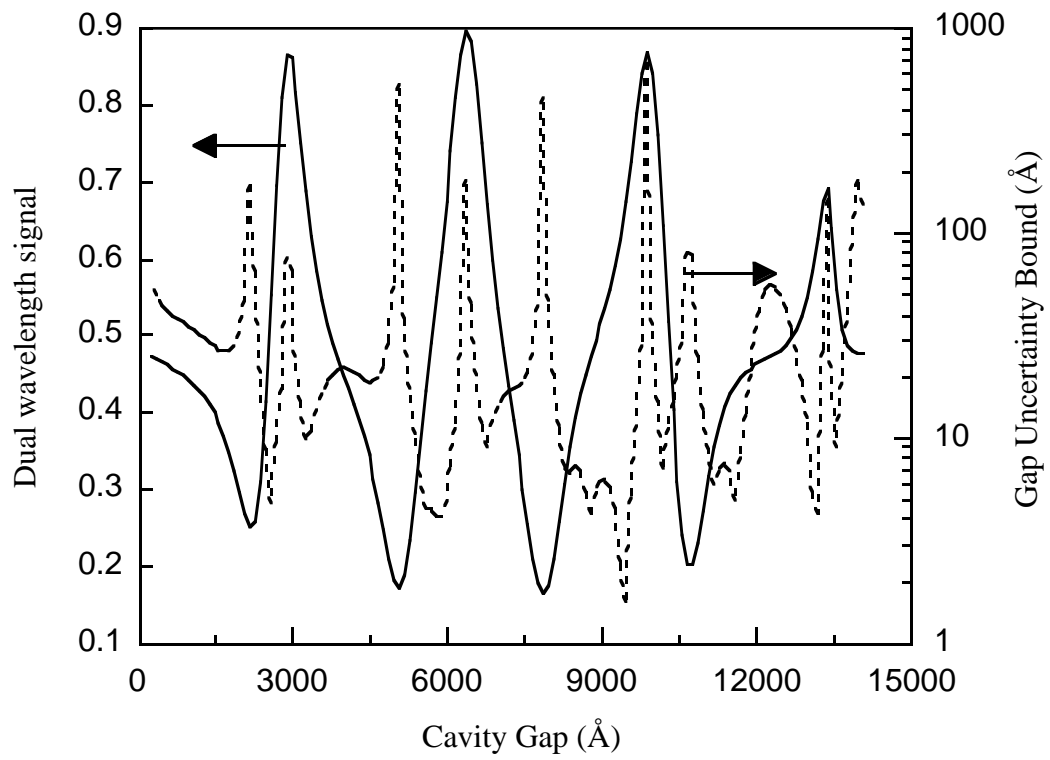
Figure 3.8 : Response curve and process-induced variations of a Fabry-Perot cavity with metal mirrors for dual wavelengths (560nm and 700nm).
Solid line: response curve; Dashed line: process-induced response variations.

Contour maps including only linear fitting-induced error indicate that an accuracy not worse than 1 % could be achieved using g_i = 6250 Å and t = 1050 Å, as shown in Figure 3.10. Note that when using dual wavelength detection linearity is maintained over a much longer travel than for single wavelength detection, as has been noted in [7] .

Figure 3.11 shows the contour plots of the error induced by both linear fitting and thickness variation for the branches with best performance. The map near 9000 Å shows that the accuracy of this branch is heavily degraded by the linear fitting-induced errors. When both errors are considered, the optimum design is g_i = 6050 Å and t = 650 Å, with at least 97 % of the manufactured sensors producing an accuracy of not worse than 3.5 %.
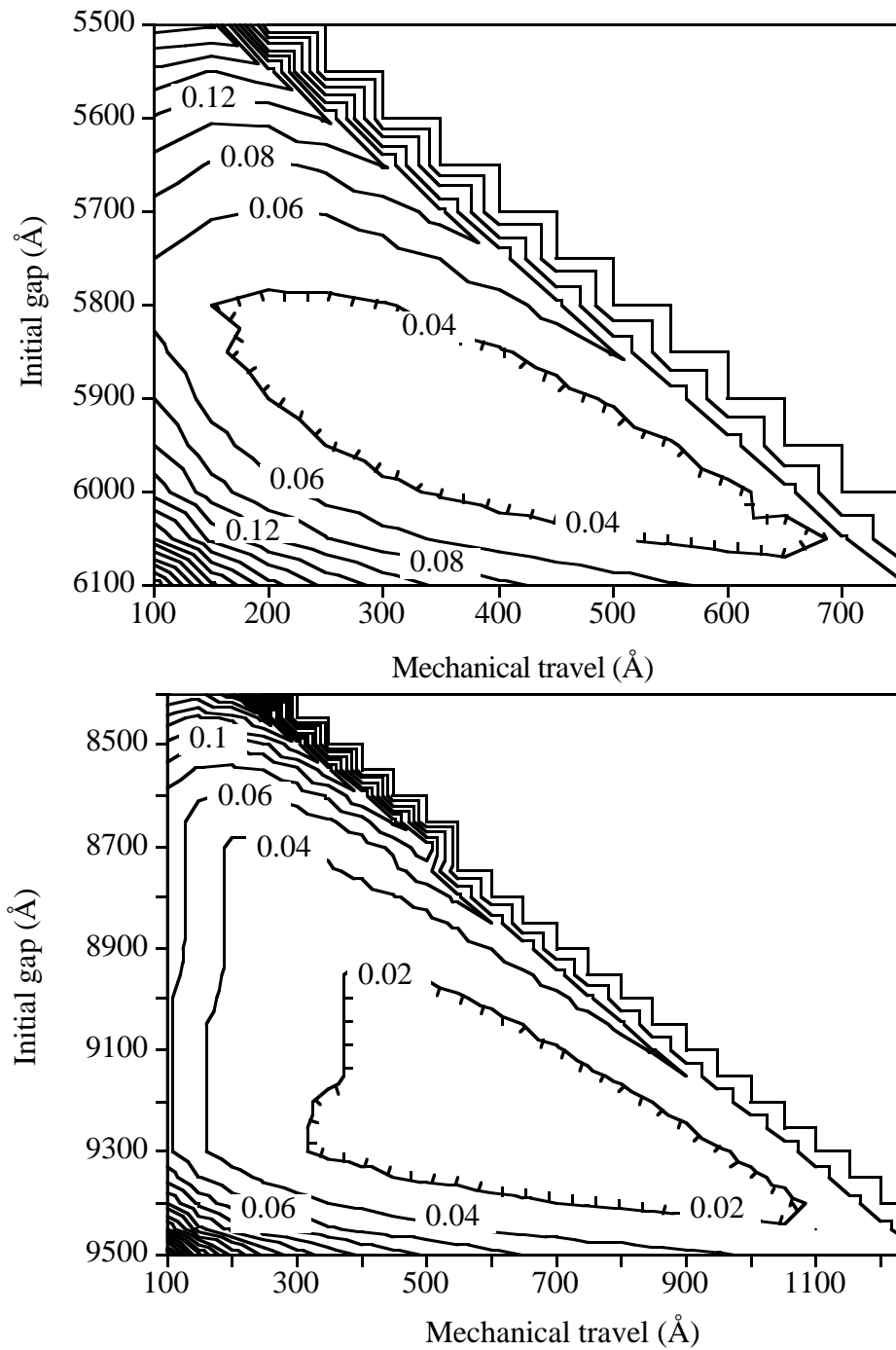
Figure 3.9 : Accuracy contour maps including only process-induced errors for two branches with best performance.
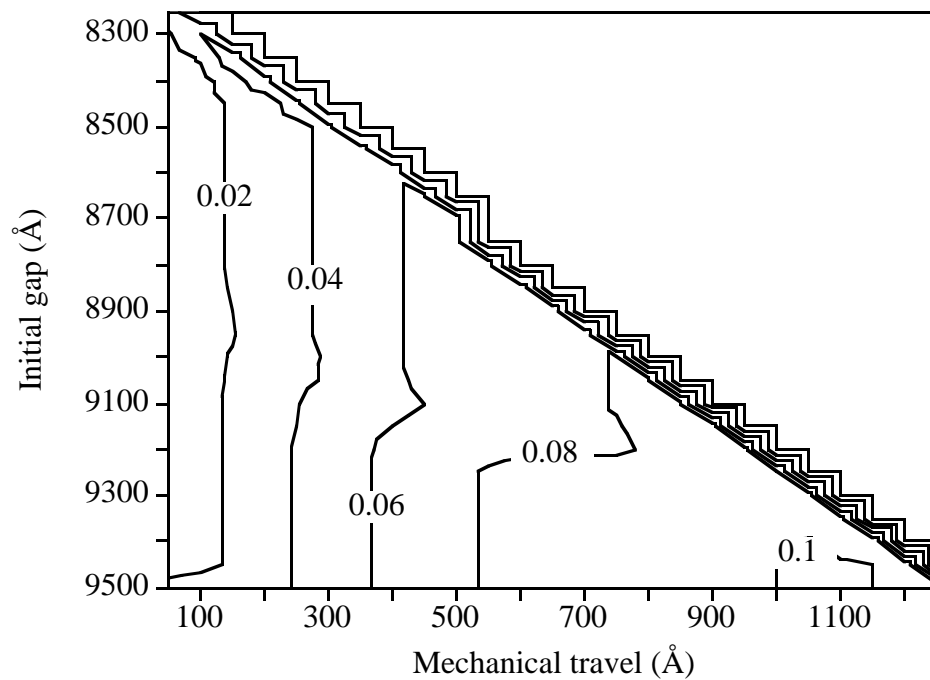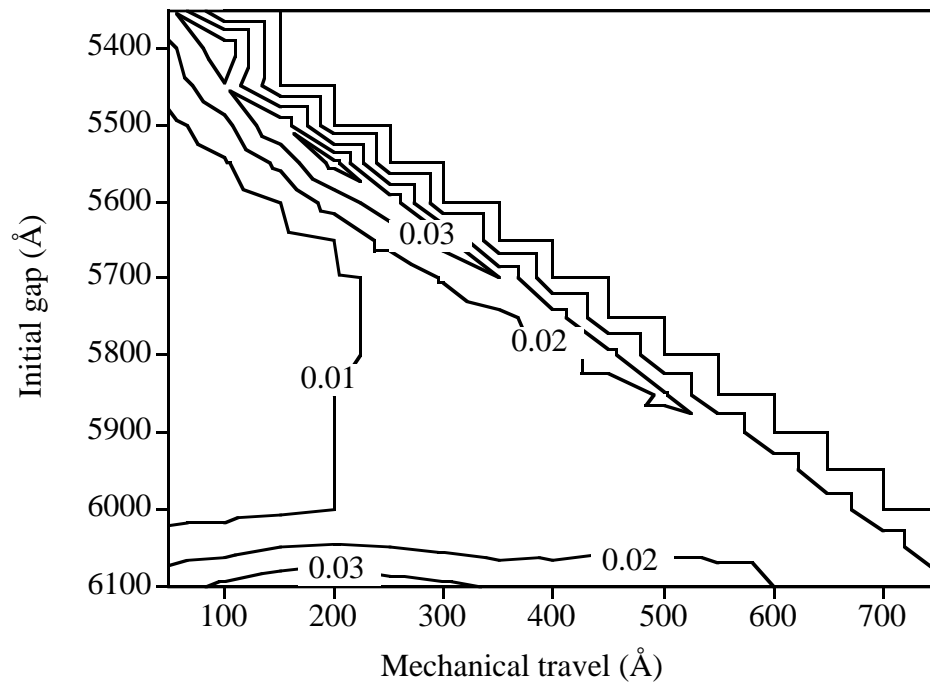
Figure 3.10 : Accuracy contour maps including linear fitting errors for two
branches with best performance.
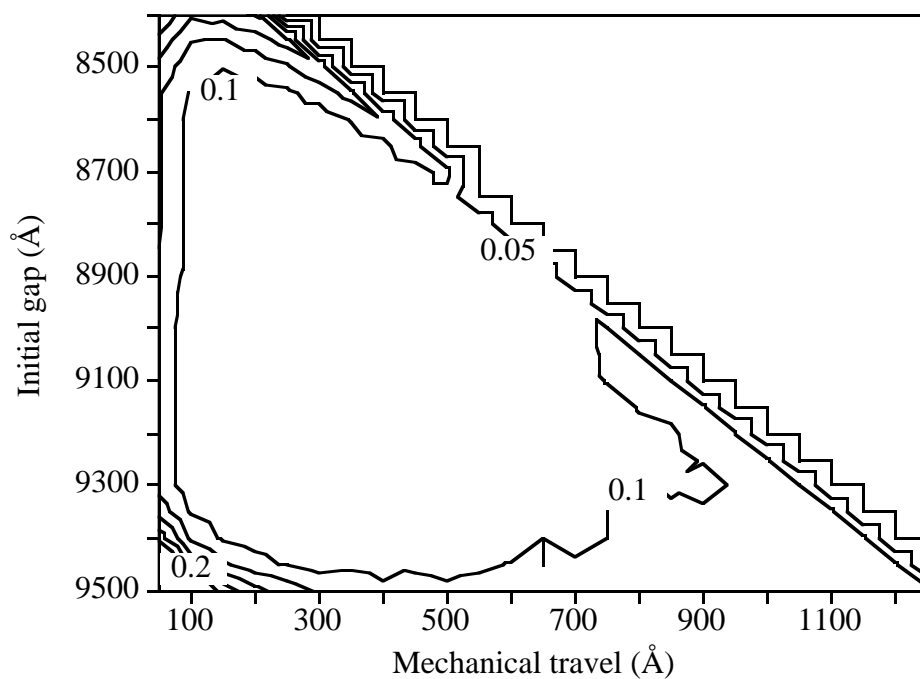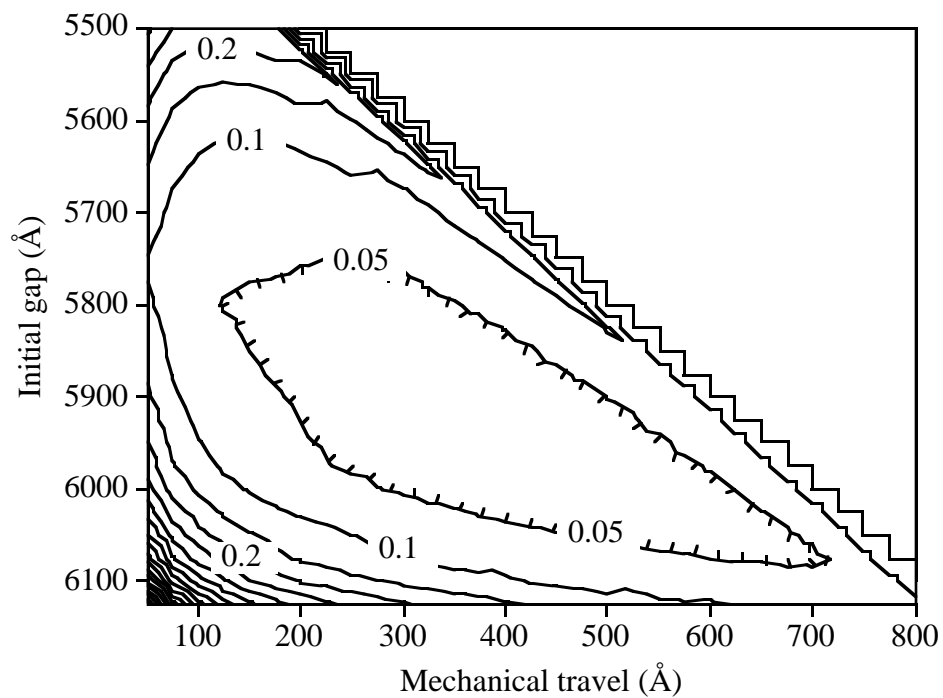
Figure 3.11 : Accuracy contour maps including both process-induced errors and linear fitting errors for two branches with best performance.

3.3 SUMMARY

The impact of thickness variations in layers on the performance of Fabry-Perot cavity sensors has been studied. It was found that for a given cavity there exists an optimum design, a combination of initial gap and mechanical travel, that gives the least variation in response curve. Through proper design high manufacturing yield with reasonable accuracy can be achieved. For the specific example of a Fabry-Perot pressure sensor discussed here, even with 3 % (three sigma) layer thickness variations, better than 5 % accuracy can be achieved from at least 97 % of the manufactured sensors by choosing the proper nominal initial gap and associated maximum mechanical travel. Also note that since a proper design is dependent on the choice of measurand, the measurand, i.e. detection method, should be determined before an optimum combination of nominal initial gap and mechanical travel is selected.

The models and design methodology discussed can also be extended easily to other sources of manufacturing variation, such as dielectric constant fluctuation. Finally, it should be straightforward to apply our approach to other interference-based micromachined devices, such as tunable interferometers [8] and modulators [9] , to find designs that minimize device sensitivity to process-induced variations.